Passivity/sliding mode control of a stand-alone hybrid generation system

F.Valenciaga, P.F.Puleston, P.E.Battaiotto and R.J.Mantz

Abstract: A novel variable structure controller for an electric generation hybrid system is proposed. The system is intended for variable alternate load and includes a wind turbine, photovoltaic generation and a battery bank. As a first step for the controller design, a dynamic model of the system is developed in a rotor reference frame. The control law is designed through the combination of passivity and sliding mode techniques. The objective is to control the operation of the wind subsystem to complement the photovoltaic generation, so the power demand is satisfied. During periods of scarce winds, the strategy is modified and the control objective becomes maximum wind generation.

1 Introduction

Electric power supply in areas isolated from the main grid can be provided by means of stand-alone systems based on renewable energy sources [1–3]. However, the variable and largely random nature of these sources, requires energy storage capabilities to ensure continuous load supply. The dimension of the storage device has an important weight in the final cost of the system. Integration of wind and photovoltaic sources, which are generally complementary, usually reduce the size of the required storage [4, 5].

There exist many different topologies of the electric generation hybrid system (EGHS). The one under consideration in this paper is presented in the schematic diagram of Fig. 1. The fixed-pitch wind turbine is directly coupled to a multipole permanent magnet synchronous generator (PMSG) which is connected, through a rectifier and a DC/DC converter, to a DC bus. The PMSG allows gearless coupling to the turbine, increasing the system robustness and efficiency [6, 7]. A photovoltaic generation subsystem is also linked to the DC bus. The bus voltage is imposed by the battery bank. Finally, a variable alternate load is fed using a static inverter.

The wind generation subsystem is a variable speed topology using a turbine without any passive blade pitching function. This means that the wind generated power and, consequently, the correspondent power injected to the DC bus, must be regulated by controlling electronically the turbine rotational speed.

The control objective is to regulate the wind power generation to satisfy the load requirements and to charge adequately the battery bank. In this paper, it is assumed that no control action is taken on the photovoltaic array. So, the power generated by this source is considered in the control design by including a known variable current injected by the solar subsystem into the DC bus. The variability of this current is due to the random nature of the solar radiation.

A reduced-order nonlinear model of the EGHS is used to design the controller, which is obtained by passivity and sliding mode control techniques. One of the most attractive features of control design based on passivity considerations is that the physical nature of the system is respected, taking advantage of the internal forces that push the system toward the sliding manifold. This results in a control law of minimum effort. In addition, its association with sliding mode techniques endows the proposed controller with robust features. The full order nonlinear model developed in Section 4 is adopted for simulation testing to validate the proficiency of the control law obtained from the reduced order model.

2 Wind turbine aerodynamics

The mechanical power captured by a wind turbine is proportional to the swept area (A), the air density (ρ), the cube of the wind speed (v) and the power coefficient (C_p). This coefficient expresses the conversion efficiency of the

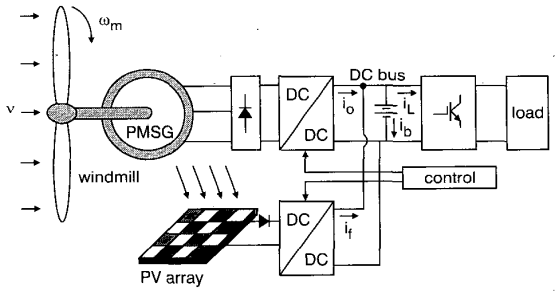

Fig. 1 *Electric generation hybrid system (EGHS)*

IEE Proceedings online no. 20000803

DOI: 10.1049/ip-cdt:20000803

Paper first received 17th April and in revised form 23rd August 2000

F. Valenciaga and P. Battaiotto are with the Laboratorio de Electrónica Industrial, Control e Instrumentación (LEICI), Facultad de Ingeniería, UNLP, La Plata, C.C. 91, C.P. 1900, Argentina

P. Puleston is with the Control and Instrumentation Group, Department of Engineering, Leicester University, LE1 7RH, England

R. Mantz is with the CICpBA, Laboratorio de Electrónica Industrial, Control e Instrumentación (LEICI), Facultad de Ingeniería, UNLP, La Plata, C.C. 91, C.P. 1900, Argentina

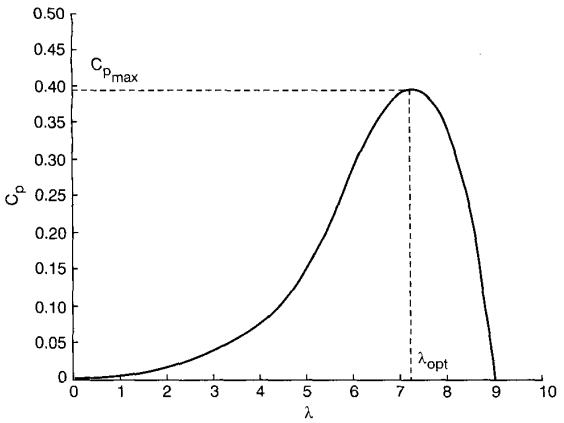

Fig. 2 *Polynomial approximation of a typical power coefficient for a horizontal axis turbine*

turbine as a function of the tip-speed ratio, which is given for:

$$\lambda = r\omega_m / v, \tag{1}$$

where

r: blade length
ω_m: angular shaft speed

Fig. 2 shows a typical profile of the power coefficient for a horizontal axis turbine. It is important to note that maximum energy capture is achieved by modifying the turbine shaft speed as the wind speed varies, to maintain $\lambda = \lambda_{opt}$.

Thus, the mechanical power generated by a turbine may be written as [8]:

$$P_t = \frac{1}{2} C_p(\lambda) \rho A v^3. \tag{2}$$

From eqn. 2, it is easy to obtain the expression of the driving torque, as

$$T_t = \frac{P_t}{\omega_m} = \frac{1}{2} C_t(\lambda) \rho A r v^2, \tag{3}$$

where $C_t(\lambda) = C_p(\lambda)/\lambda$ is the torque coefficient of the turbine.

3 Wind subsystem modelling

In this Section, only the fundamental components of the electrical variables are considered for the analysis.

3.1 Static analysis

As it is shown in Fig. 1, the turbine is linked to the battery bank through a diode bridge rectifier and a DC/DC converter. This configuration presents a pure active power load to the generator terminals ($\cos(\varphi) = 1$), whose value can be modified through the duty cycle (δ) of the converter. A per-phase phasor diagram of the PMSG electrical variables is presented in Fig. 3. In this picture, E_f corresponds to the EMF in the stator windings, R_s is the synchronous resistance, X_s is the synchronous reactance and V_s and I_s are the line voltage and current on the PMSG terminals respectively. It is important to note that the voltage V_s is externally imposed by the DC/DC converter, i.e. it is a function of δ.

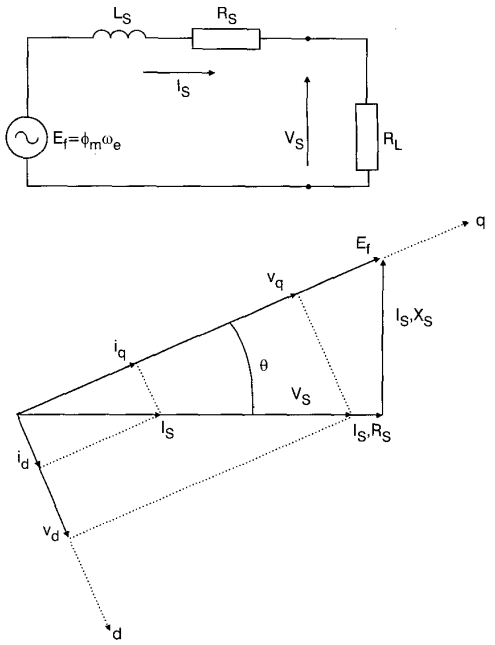

Fig. 3 *Per-phase circuit and phasor diagram of the PMSG*

Neglecting the voltage drop in the synchronous resistance, the electrical load torque produced by the PMSG can be written as follows [9]:

$$T_e = \frac{3PV_s\phi_m}{4\omega_e L_s}\sqrt{1 - \left(\frac{V_s}{\omega_e \phi_m}\right)^2}, \tag{4}$$

with

P: number of poles
$\omega_e = (P/2)\omega_m$: electrical angular speed
ϕ_m: flux linked by the stator windings

It is interesting to note that for a given constant voltage in the PMSG terminals (V_s), there exists a minimum shaft speed below which the system cannot generate. This lower limit arises naturally from the analysis of the phasor diagram depicted in Fig. 3, since it cannot be built for speeds that induce E_f smaller than V_s. The expression of the electrical angular speed corresponding to that limit can be obtained from (4):

$$\omega_{e_{lim}} = V_s/\phi_m. \tag{5}$$

Fig. 4 shows, in dashed lines, the turbine torque curves (T_t) in function of the angular shaft speed, parameterised in

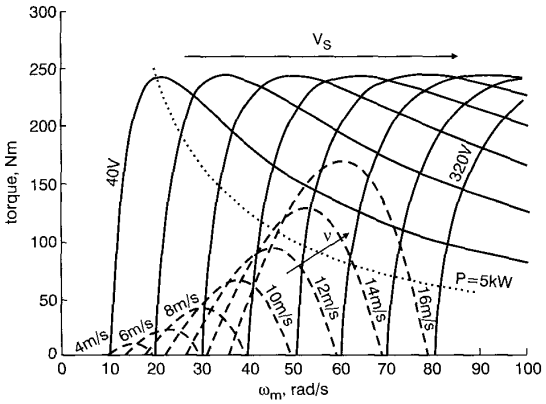

Fig. 4. *Turbine and PMSG torque-shaft speed curves*

terms of the wind speed. The torque curves of the PMSG (T_e) are presented as solid lines. In this case, they are parameterised in function of V_s. The intersection points between T_e and the horizontal axis correspond to the theoretical speed limit of generation. Finally, the nominal power of the PMSG is depicted in dotted line.

3.2 Dynamic analysis

The PMSG dynamic model in a rotor reference frame is given by the following equations [10]:

$$v_q = -R_s i_q - L_q s i_q - \omega_e L_q i_d + \omega_e \phi_m \tag{6}$$

$$v_d = -R_s i_d - L_d s i_d + \omega_e L_d i_q \tag{7}$$

$$T_e = \frac{3}{2}\frac{P}{2}(\phi_m i_q + (L_d - L_q) i_q i_d), \tag{8}$$

with:

L_q, L_d: stator inductances in the d-q axes
s: Laplace operator.

Using the phasor diagram of Fig. 3, eqns. 6 and 7 may be expressed in terms of the terminal generator voltage, as:

$$\frac{V_s i_q}{\sqrt{i_q^2 + i_d^2}} = -R_s i_q - L_q s i_q - \omega_e L_q i_d + \omega_e \phi_m \tag{9}$$

$$\frac{V_s i_d}{\sqrt{i_q^2 + i_d^2}} = -R_s i_d - L_d s i_d + \omega_e L_d i_q. \tag{10}$$

Furthermore, in actual radial flux PMSGs with a smooth airgap it holds $L_d \cong L_q \cong L_s \cong L$ [10, 11], therefore eqn. 8 reduces to:

$$T_e = \frac{3}{2}\frac{P}{2}\phi_m i_q. \tag{11}$$

As was previously said the voltage in the PMSG terminals can be controlled by modifying the duty cycle of the DC/DC converter. Voltage V_s is described by the following expression:

$$V_s = \frac{\pi v_b}{3\sqrt{3}} u_x, \tag{12}$$

where v_b is the voltage of the DC bus and u_x is a simple function of the DC/DC converter duty cycle δ (in this particular topology $u_x = k_{tr}/\delta$, with k_{tr} the winding ratio of the transformer included in the DC/DC converter). Thus, using eqn. 12, eqns. 9 and 10 can be rewritten as:

$$\dot{i}_q = -\frac{R_s}{L} i_q - \omega_e i_d + \frac{\omega_e \phi_m}{L} - \frac{\pi v_b i_q u_x}{3\sqrt{3} L \sqrt{i_q^2 + i_d^2}} \tag{13}$$

$$\dot{i}_d = -\frac{R_s}{L} i_d - \omega_e i_q - \frac{\pi v_b i_d u_x}{3\sqrt{3} L \sqrt{i_q^2 + i_d^2}}. \tag{14}$$

Besides, assuming an ideal static conversion, the output current of the DC/DC converter can be readily determined equating its input and output power. This yields:

$$i_o = \frac{\pi}{2\sqrt{3}} \sqrt{i_q^2 + i_d^2}\, u_x. \tag{15}$$

Thus, the dynamic model of the wind subsystem is described by eqns. 11, 13, 14 and 15.

4 Dynamic model of the EGHS

As can be seen in Fig. 1, all subsystems are linked to the DC bus. Thus, their concurrent effects can be easily analysed by considering their currents in the common DC side. In this way, assuming an ideal voltage inverter, the load current can be referred to the DC side as an output variable current i_L. On the other hand, the operation of the photovoltaic panels may be represented by a variable current injected in the bus, denoted as i_f. Therefore, the current across the battery bank can be written as:

$$i_b = \frac{\pi}{2\sqrt{3}} \sqrt{i_q^2 + i_d^2}\, u_x + i_f - i_L, \tag{16}$$

where i_f and i_L are easy to measure and, thus, assume to be known currents.

The lead-acid battery bank may be modelled as a voltage source E_b connected in series with a resistance R_b and a capacitance C_b [11]. Based on this simple model and eqn. 16, the DC bus voltage expression results:

$$v_b = E_b + v_c + \left(\frac{\pi}{2\sqrt{3}} \sqrt{i_q^2 - i_d^2}\, u_x + i_f - i_L\right) R_b, \tag{17}$$

where v_c is the voltage in capacitor C_b.

Thus, from eqns. 11, 13, 14 and 15, along with the dynamic equations of the mechanical rotational system and the battery bank, the whole dynamic model of the EGHS can be written as

$$\dot{i}_q = -\frac{R_s}{L} i_q - \omega_e i_d + \frac{\omega_e \phi_m}{L} - \frac{\pi v_b i_q u_x}{3\sqrt{3} L \sqrt{i_q^2 + i_d^2}} \tag{18a}$$

$$\dot{i}_d = -\frac{R_s}{L} i_d - \omega_e i_q - \frac{\pi v_b i_d u_x}{3\sqrt{3} L \sqrt{i_q^2 + i_d^2}} \tag{18b}$$

$$\dot{\omega}_e = \frac{P}{2J}\left(T_t - \frac{3}{2}\frac{P}{2}\phi_m i_q\right) \tag{18c}$$

$$\dot{v}_c = \frac{1}{C_b}\left(\frac{\pi}{2\sqrt{3}} \sqrt{i_q^2 + i_d^2}\, u_x + i_f - i_L\right). \tag{18d}$$

where J is the inertia of the rotating system and v_b is given by eqn. 17. Note that in the mechanical rotational dynamics (eqn. 18c), the friction term is neglected.

5 Control strategy

5.1 Controller design

The primary objective is to control the current injected by the wind subsystem into the DC bus (i_o), to complement that injected by the photovoltaic subsystem, and to satisfy the power demand. The demand comprises the external load and the battery charge requirements, which vary according to the state of charge of the battery bank. In this way, during wind regimes of full generation, the system can meet the load requirements and store energy to be used in periods of scarce generation.

The control law is designed from a unified theoretical framework, assembling passivity and sliding mode control techniques. The use of these techniques is suitable for configurations employing switched power converters [12], as the one presently studied, and also has many attractive properties. For example, the formulation from passivity results in a control that respects the physical nature of the system by maintaining the internal forces that push the system towards the sliding manifold. That is, the control is only used to cancel the undesirable internal forces that draw the system apart from the sliding manifold. Thus, a

minimal effort control law is attained [13], allowing to reduce the chattering effect characteristic of sliding mode controlled systems. In addition, the use of sliding mode control techniques endows the proposed strategy with robustness.

A reduced-order model is used for the control design. The full model described by eqn. 18 was reduced under some practical assumptions. Their validity was confirmed by adopting the fully nonlinear description of the system for simulation testing. Besides, it was also established that the control design based on the reduced-order model does not introduce significant errors in the cancellation of the undesirable internal forces. The assumptions used for the control design were:

(i) Mechanical rotational dynamics are slower than electrical dynamics. This condition verifies in most wind energy conversion systems.
(ii) Inside the operation area (see Fig. 4), delimited by the maximum and minimum wind speed and the PMSG nominal power, the electrical torque admits a linear representation. Thus, the PMSG electrical torque can be written as:

$$T_{e_{lin}} = K(\omega_e - \omega_{e_{lim}}) = \frac{3P\phi_m^2}{4R_s}\left(\omega_e - \frac{\pi v_b u_x}{3\sqrt{3}\phi_m}\right), \quad (19)$$

where the coefficient K is obtained by taking the derivative of the exact electrical torque equation with respect to the electrical speed, over the limit speed point ($\omega_{e_{lim}}$). The exact expression of the torque can be obtained by equating eqns. 9 and 10 to zero and substituting in eqn. 11.
(iii) The terminals voltage of the battery bank can be considered constant, i.e. v_b variations, due to abrupt load demand or battery recharge, are neglected.

Under these conditions the full order model given in eqn. 18 reduces to:

$$\dot{\omega}_e = \frac{P}{2J}\left(\frac{1}{2}C_t(\lambda)\rho A r v^2 - \frac{3P\phi_m^2\omega_e}{4R_s} + \frac{\pi P\phi_m v_b u_x}{4\sqrt{3}R_s}\right). \quad (20)$$

The sliding variable h_1 can be written in terms of the system currents:

$$h_1 = I_{o_{ref}} - i_o = I_{b_{ref}} + i_L - i_f - i_o, \quad (21)$$

where $I_{b_{ref}}$ is the reference charge current of the battery bank, which varies according with its state of charge. Then, the sliding manifold, that satisfies the control objective, is determined by $h_1 = 0$.

After routine algebraic manipulations with eqns. 4, 11, 15, 19 and 21, h_1 can be expressed as:

$$h_1 = I_{b_{ref}} + i_L - i_f - \frac{\pi u_x}{2\sqrt{3}}\left\{\left(\frac{\phi_m\omega_e}{R_s} - \frac{\pi v_b u_x}{3\sqrt{3}R_s}\right)^2 + \frac{\left(\phi_m - \left(\phi_m^2 - 4L^2\left(\frac{\phi_m\omega_e}{R_s} - \frac{\pi v_s u_x}{3\sqrt{3}R_s}\right)^2\right)^{\frac{1}{2}}\right)^2}{4L^2}\right\}^{\frac{1}{2}}. \quad (22)$$

Up to this point, the control signal of the system is u_x. However, injecting a switched control signal through this input produces undesirable wide variations in T_e. This results in a high ripple on the current of the DC/DC converter (i_o). To avoid this problem, a dynamic extension is proposed, including an integrator previous to the input u_x. Then, u_x becomes a new state variable and the integrated signal (w) the new input to the system. In this way, the switched control signal is filtered, reducing the ripple [14]. In addition, it breaks the algebraic dependence between the sliding manifold and the input of the system. Hence, the switching surface turns to be of relative degree one and verifies the transversality condition in the whole operation area. Thus, the dynamic model of the extended system is:

$$\dot{\boldsymbol{x}} = \begin{bmatrix}\dot{\omega}_e \\ \dot{u}_x\end{bmatrix} = \boldsymbol{f}(\boldsymbol{x}) + \boldsymbol{g}(\boldsymbol{x})w = \begin{bmatrix}f_1(\boldsymbol{x}) \\ f_2(\boldsymbol{x})\end{bmatrix} + \begin{bmatrix}g_1(\boldsymbol{x}) \\ g_2(\boldsymbol{x})\end{bmatrix}w = \begin{bmatrix}\frac{P}{2J}(T_t - T_{e_{lin}}) \\ 0\end{bmatrix} + \begin{bmatrix}0 \\ 1\end{bmatrix}w \quad (23)$$

where the state vector is $\boldsymbol{x} = [\omega_e \quad u_x]^T$.

To design a sliding mode control based on passivity concepts, the following positive semidefinite energy function is defined:

$$V(\boldsymbol{x}) = \frac{1}{2}h_1(\boldsymbol{x})^2, \quad (24)$$

Considering this definition, the dynamical model of the system may be written in the passivity based control canonical form [15], as:

$$\dot{\boldsymbol{x}} = \boldsymbol{J}(\boldsymbol{x})\frac{\partial \boldsymbol{h}_1}{\partial \boldsymbol{x}} + \boldsymbol{Q}(\boldsymbol{x})\frac{\partial \boldsymbol{h}_1}{\partial \boldsymbol{x}} + \boldsymbol{g}(\boldsymbol{x})w, \quad (25)$$

where $\boldsymbol{Q}(\boldsymbol{x}) = \boldsymbol{Q}(\boldsymbol{x})^T$ and $\boldsymbol{J}(\boldsymbol{x}) = -\boldsymbol{J}(\boldsymbol{x})^T$, and are given by:

$$\boldsymbol{J}(\boldsymbol{x}) = \frac{1}{2L_g h_1(\boldsymbol{x})}[\boldsymbol{f}(\boldsymbol{x})\boldsymbol{g}^T(\boldsymbol{x}) - \boldsymbol{g}(\boldsymbol{x})\boldsymbol{f}^T(\boldsymbol{x})] \quad (26)$$

$$\boldsymbol{Q}(\boldsymbol{x}) = \frac{1}{2L_g h_1(\boldsymbol{x})}[\boldsymbol{f}(\boldsymbol{x})\boldsymbol{g}^T(\boldsymbol{x}) - \boldsymbol{g}(\boldsymbol{x})\boldsymbol{f}^T(\boldsymbol{x})]. \quad (27)$$

Splitting $\boldsymbol{Q}(\boldsymbol{x})$ into two matrices according to the sign of its eigenvalues, that is into a positive semidefinite matrix $\boldsymbol{P}(\boldsymbol{x})$ and a negative semidefinite matrix $\boldsymbol{N}(\boldsymbol{x})$, eqn. 25 becomes:

$$\dot{\boldsymbol{x}} = \boldsymbol{J}(\boldsymbol{x})\frac{\partial \boldsymbol{h}_1}{\partial \boldsymbol{x}} + \boldsymbol{P}(\boldsymbol{x})\frac{\partial \boldsymbol{h}_1}{\partial \boldsymbol{x}} - \boldsymbol{N}(\boldsymbol{x})\frac{\partial \boldsymbol{h}_1}{\partial \boldsymbol{x}} + \boldsymbol{g}(\boldsymbol{x})w, \quad (28)$$

From eqn. 28, it is straighforward to calculate:

$$\dot{V} = h_1(\boldsymbol{x})\underbrace{\left[\frac{\partial \boldsymbol{h}_1}{\partial \boldsymbol{x}^T}\boldsymbol{J}(\boldsymbol{x})\frac{\partial \boldsymbol{h}_1}{\partial \boldsymbol{x}} + \frac{\partial \boldsymbol{h}_1}{\partial \boldsymbol{x}^T}\boldsymbol{P}(\boldsymbol{x})\frac{\partial \boldsymbol{h}_1}{\partial \boldsymbol{x}} + \frac{\partial \boldsymbol{h}_1}{\partial \boldsymbol{x}^T}\boldsymbol{N}(\boldsymbol{x})\frac{\partial \boldsymbol{h}_1}{\partial \boldsymbol{x}} - \frac{\partial \boldsymbol{h}_1}{\partial \boldsymbol{x}^T}\boldsymbol{g}(\boldsymbol{x})w\right]}_{(F)}. \quad (29)$$

Analysing factor (F) of eqn. 29, it can be seen that its first term is identically null since $\boldsymbol{J}(\boldsymbol{x})$ is an antisymmetric matrix. Besides, the second and the third terms are always positive and negative semidefinite, respectively. Thus, depending on the sign of $h_1(\boldsymbol{x})$, one of these terms will contribute to lead the system toward the sliding manifold, while the other will lead the system away from it. The fourth term represents the energy externally injected through the control signal w. To force the system to cross

the sliding manifold and to operate in sliding mode, this fourth term can be used to cancel the undesirable contribution of either the second term or the third term of factor (F). Then, a switched control law arises naturally, as follows:

$$w = \begin{cases} w_1^+ = \dfrac{-1}{L_g h_1(x)} \left[\dfrac{\partial h_1}{\partial x^T} P(x) \dfrac{\partial h_1}{\partial x} \right] & \text{if } h_1(x) \geq 0 \\ w_1^- = \dfrac{-1}{L_g h_1(x)} \left[\dfrac{\partial h_1}{\partial x^T} N(x) \dfrac{\partial h_1}{\partial x} \right] & \text{if } h_1(x) \leq 0. \end{cases} \tag{30}$$

That is:

$$w^+ = \frac{-|f_1(x)|}{4} \times \left[\frac{-18L^2\phi_m^2 u_x \omega_e + 2\pi\sqrt{3}L^2 u_x^2 \phi_m \mathrm{v}_b}{\sqrt{3D}\phi_m R_s + 9\phi_m^2 R_s^2 - 36C + 10B - 2A} + 1 \right]^2 \tag{31a}$$

$$w^- = \frac{|f_1(x)|}{4} \times \left[\frac{18L^2\phi_m^2 u_x \omega_e - 2\pi\sqrt{3}L^2 u_x^2 \phi_m \mathrm{v}_b}{\sqrt{3D}\phi_m R_s + 9\phi_m^2 R_s^2 - 36C + 10B - 2A} + 1 \right]^2. \tag{31b}$$

where

$$A = \pi^2 L^2 \mathrm{v}_b^2 u_x^2$$
$$B = \pi\sqrt{3}L^2 \mathrm{v}_b \phi_m \omega_e u_x$$
$$C = L^2 \phi_m^2 \omega_e^2$$
$$D = 27\phi_m^2 R_s^2 - 108C + 24B - 4A.$$

5.2 Controller operation during insufficient wind regimes

It happens that, during insufficient wind regimes, the maximum energy captured from the wind is not enough to satisfy the load and battery bank requirements. So, the system is not able to operate on the sliding manifold determined by h_1 and, consequently, it can be stuck in operating points of no electrical generation. This undesirable situation can be illustrated by means of the schematic diagram of Fig. 5. It shows the turbine torque characteristic (parameterised in terms of the wind speeds $v_1 > v_2$) and the electrical torque corresponding to the sliding surface h_1 (for a given DC/DC output current (i_s)). Also, the curve of maximum wind power generation is depicted (dotted line). Initially, the system operates at point A, with speed v_1 (sufficient wind regime). Then, an abrupt fall of the wind speed, from v_1 to v_2, is assumed (insufficient wind regime). The inertia does not permit an instantaneous change in the rotational speed, so the turbine torque turns to be that of point B. Due to this reduction, the speed diminishes and h_1 becomes positive. Hence, according to eqn. 30, the control is the negative signal w^+. However, it can be observed that, even reducing the speed, the increase of the turbine torque is still insufficient. Therefore, u_x, will continuously decrease, eventually driving the turbine to stall.

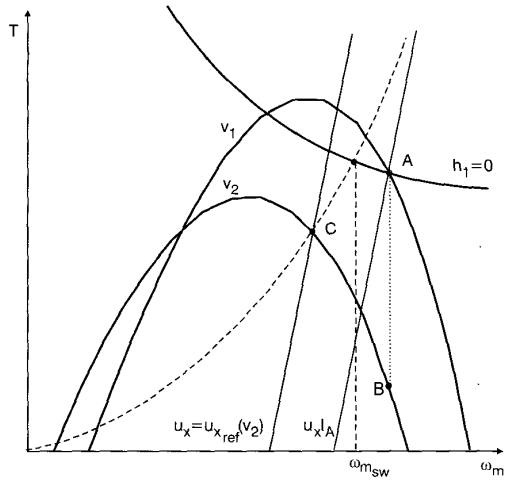

Fig. 5. *Schematic behaviour of the system in the torque-speed plane*

Incorporating a second sliding surface, which operates during insufficient wind regimes, can solve this problem. The objective is to extract the maximum power available in the wind, i.e. to operate in the maximum generation points. Then, the proposed secondary sliding surface is:

$$h_2 = u_{xref} - u_x \tag{32}$$

$$w = \begin{cases} w_2^+ & \text{if } h_2(x) \geq 0 \\ w_2^- & \text{if } h_2(x) \leq 0 \end{cases}, \quad w_2^+ > 0 \text{ and } w_2^- < 0 \tag{33}$$

The reference u_{xref} determines the values of u_x that correspond maximum wind power generation. It is a function of the wind speed and can be obtained from eqns. 3 (evaluated for $\lambda = \lambda_{opt}$) and 19:

$$u_{xref} = \frac{3\sqrt{3}\phi_m}{\pi \mathrm{v}_b} \left(\frac{\lambda_{opt} v P}{2r} - \frac{2R_s C_t(\lambda_{opt}) \rho A r v^2}{3P\phi_m^2} \right). \tag{34}$$

The application of this second surface drives the system to operate at point C after the abrupt wind speed fall.

The decision about which sliding surface must operate can be easily taken. It is possibly to obtain the expression of the boundary speed (ω_{mSW}) between sufficient and insufficient wind regimes by equating the maximum wind power with the power demand, resulting:

$$\omega_{mSW} = \sqrt[3]{\frac{I_{oref} \mathrm{v}_b}{K}}, \tag{35}$$

where $K = C_t(\lambda_{opt}) \rho A r^3 / 2\lambda_{opt}^2$.

Then

$$\begin{cases} \text{if } \omega_m \geq \omega_{mSW} & \text{Sliding Surface } h_1 : \text{ sufficient wind regimes} \\ \text{if } \omega_m \leq \omega_{mSW} & \text{Sliding Surface } h_2 : \text{ insufficient wind regimes} \end{cases} \tag{36}$$

Finally, it is important to note that in eqn. 33, for simplicity, w_2^+ and w_2^- have been assumed to be constants. However, they can also be designed based on passivity considerations, in a similar manner to w_1^+ and w_1^-, as was described in Subsection 5.1.

6 Simulation results

Computer simulations were conducted to evaluate the performance of the proposed controller. The plant was modelled with the comprehensive full order model detailed in eqn. 18. The parameter values used for the simulations are given in the Appendix A.

The features of the proposed control are examined through two examples. Example A aims to show the performance of the control strategy during sufficient wind regimes, while example B is intended to analyse its behaviour when insufficient wind regimes occur.

6.1. Example A. Operation during sufficient wind regimes

In Figs. 6*a*, 6*b*, 7*a* and 7*b*, the time evolution of the external variables can be observed. Fig. 6*a* shows the wind speed signal (v) varying between 8 m/s and 13 m/s, with a mean of 10.8 m/s. This profile was generated by adding two signals which characterise the turbulent part of the wind and its slow variations, respectively. Fig. 6*b*

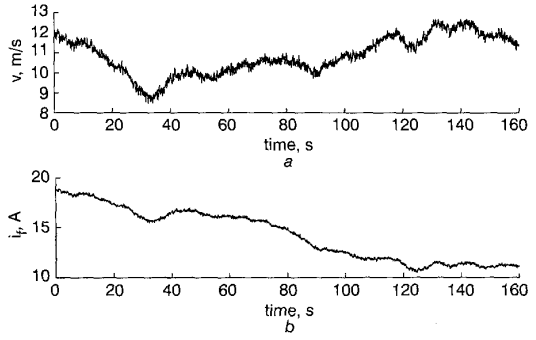

Fig. 6. *Photovoltaic subsystem*

a Wind speed
b Current injected in the DC bus by the photovoltaic subsystem i_f

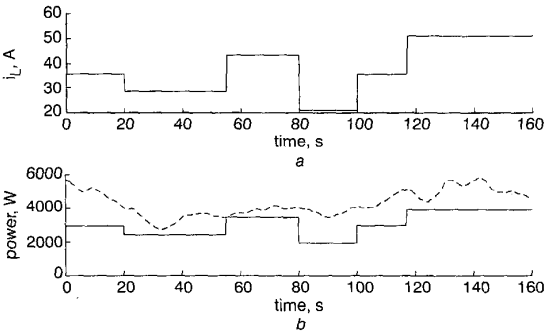

Fig. 7. *Generation*

a Load current referred to the DC bus side i_L
b Power demand and maximum power available for generation (dashed line)

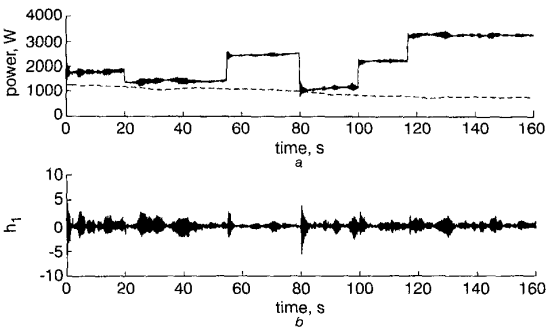

Fig. 8. *System operation*

a Power generated by the wind subsystem (solid line) and by the solar subsystems (dashed line)
b Sliding variable h_1

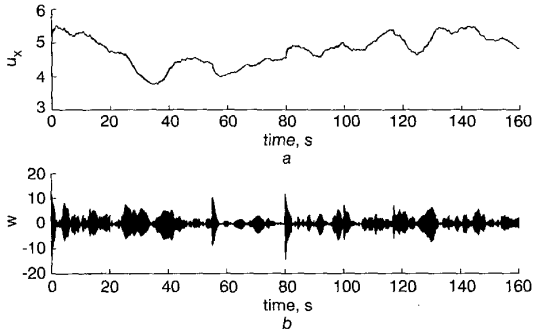

Fig. 9. *System operation*

a Duty cycle function of the DC/DC converter u_x
b Control action w

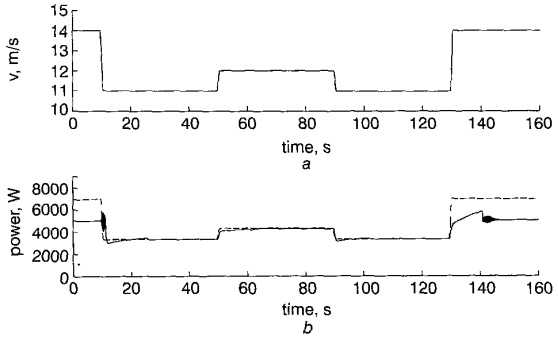

Fig. 10. *System operation*

a Wind speed
b Power generated by the wind subsystem and maximum wind power available for generation (dashed line)

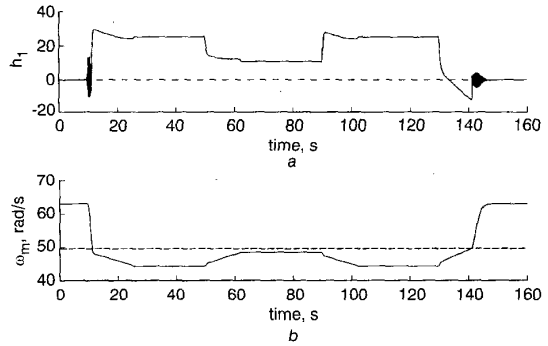

Fig. 11. *System operation*

a Sliding variable h_1
b Shaft angular speed (solid line) and ω_{mSw} (dashed line)

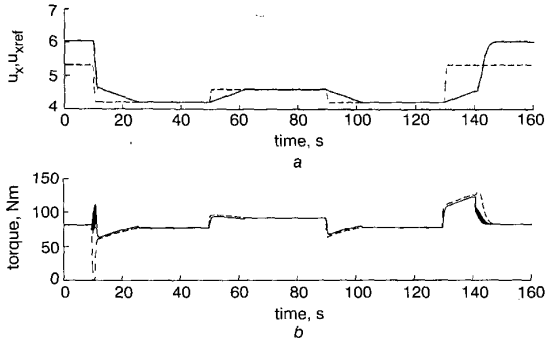

Fig. 12. *System operation*

a Duty cycle function of the DC/DC converter u_x (solid line) and reference value u_{xref} (dashed line)
b Electrical torque (solid line) and turbine torque (dashed line)

displays the current injected in the DC bus by the photovoltaic subsystem (i_f). This sequence was generated similarly to the wind speed, assuming a 1500 W PV array. Fig. 7*a* depicts the load current referred to the DC bus side (i_L). The steps in this profile take into account abrupt load connection or disconnection. Fig. 7*b* shows the power demand (load + battery) and the maximum power available for generation (photovoltaic + wind) in dashed line.

In Figs. 8*a*, 8*b*, 9*a* and 9*b*, the time behaviour of different variables of the system is depicted. In Fig. 8*a*, the power generated by the wind and photovoltaic subsystems are displayed. The step-like shape of the wind generated power is due to the tracking of the load demand. It can be observed that the wind subsystem is complementing the photovoltaic generation. In Fig. 8*b*, the evolution of the sliding variable h_1 is displayed. Finally, in Figs. 9*a* and 9*b*, the signal u_x and the control signal w are plotted, respectively. Note the adaptation of the switching control values w_1^+ and w_1^-, owing to the design based on passivity considerations. It is important to remark that such minimum effort switching control law results in a chattering reduction of the output current of the DC/DC converter.

6.2 Example B. Operation during insufficient wind regimes

In this example, periods of sufficient and insufficient wind regimes are alternated. For clarity, the photovoltaic power was assumed to be zero ($i_f = 0$) and the power demand was assumed constant (5000 W). A step series of wind speed (Fig. 10*a*) was chosen to illustrate this mode of operation. Speeds of 11 ms and 12 m/s represent the insufficient wind regimes, while the sufficient wind regimes are represented by $v = 14$ m/s.

Initially, the system is operating in a sufficient wind regime ($v = 14$ m/s) and consequently, it slides over the surface h_1 (see Figs. 10*b* and 11*a*). At time 10 s, an abrupt reduction in the wind speed occurs and the wind becomes insufficient. For a short period, the wind subsystem can deliver the demanded power, by making use of the energy stored in its inertia. Obviously, this is at the expense of a rotational speed reduction. If this situation continued, then the turbine would stall. However, shortly after 11.1 s, the rotational speed crosses the boundary speed ω_{mSw} (Fig. 11*b*) and the secondary sliding control (given by eqns. 32 and 33) takes charge. Then, after a reaching time, the secondary sliding surface (h_2) is attained (see in Fig. 12*a*, when u_x reaches u_{xref}), and maximum power is extracted from the wind (see Fig. 10*b*). The reaching time depends on the tuning of the switching control values w_2^+ and w_2^-. In this example, they were selected $w_2^+ = 0.03$ and $w_2^- = -0.03$, considering for the design, the trade-off between the length of reaching time and the size of the battery current peaks. Finally, in Fig. 12*b*, the time evolution of the electrical torque and the turbine torque are displayed.

7 Conclusions

A dynamic model of a stand-alone hybrid generation system was developed. The system comprises a wind-driven permanent magnet synchronous generator, photovoltaic array and a battery bank. A reduced-order nonlinear model was used for control design based on passivity and sliding mode control techniques. Such combination resulted in a minimum effort control law with robust features. An additional advantage of the minimum effort nature of the control is the chattering reduction of the DC/DC converter output current.

To cope with insufficient wind regimes, a secondary sliding surface was incorporated. Its objective was to extract the maximum power available in the wind. This was achieved by using a variable reference for the control input of the DC/DC converter. The activation of this secondary sliding surface was readily determined from speed and current measurements.

The proficiency of the proposed controller was assessed through computer simulations, by controlling satisfactorily a comprehensive full-order model of the plant.

8 Acknowledgments

Dr. P.F. Puleston is on leave from CONICET and LEICI, Dept. Electrotecnia, Facultad de Ingeniería, UNLP, Argentina.

9 References

1 BOROWY, B.S., and SALAMEH, Z.M.: 'Methodology for optimally sizing the combination of a battery bank and PV array in a wind/PV hybrid system', *IEEE Trans. Energy Convers.*, 1996, **11**, (2), pp. 367–375
2 NAYAR, C.: 'Novel wind/diesel/battery hybrid energy systems', *Solar Energy*, 1993, **51**, pp. 65–78
3 UHLEN, K., FOSS, B.A., and GJØSÆTER, O.B.: 'Robust control and analysis of a wind-diesel hybrid power plant', *IEEE Trans. Energy Convers.*, 1994, **9**, (4), pp. 701–708
4 CHALMERS, B.J., WU, W., and SPOONER, E: 'An axial-flux permanent-magnet generator for a gearless wind energy system', *IEEE Trans. Energy Convers.*, 1999, **14**, (2), pp. 251–257
5 JAYADEV, J.: 'Harnesing the wind', *IEEE Spectr.*, 1995, **32**, (11), pp. 78–83
6 SÖDERLUND, L., ERIKSSON, J.T., SALONEN, J., VIHRIÄLÄ, H., and PERÄLÄ, R.: 'A permanent-magnet generator for wind power applications', *IEEE Trans. Mag.*, 1996, **32**, (4), pp. 2389–2392
7 GRAUERS, A.: 'Efficiency of three wind energy generator systems', *IEEE Trans. Energy Convers.*, 1996, **11**, (3), pp. 650–656
8 CAVALLO, A.J., HOCK, S.M., and SMITH, D.R.: 'Wind energy, renewable energy: Sources for fuels and electricity' (T.B. Johanson et al. Island Press, Washington D.C., 1993, 1st edn.)
9 MULJADI, E., DROUILHET, S., HOLZ, R., and GEVORGIAN, V.: 'Analysis of wind ower for battery charging'. Fifteenth ASME Wind energy symposium, January 1996, Huston, TX, US
10 KRAUSE, P.C., WASYNCZUK, O., and SUDHORFF, S.D.: 'Analysis of electric machinery' (IEEE Press, New York, 1995, 1st edn.)
11 BOROWY, B.S., and SALAMEH, Z.M.: 'Dynamic response of a stand-alone wind energy conversion system with battery energy storage to a wind gust', *IEEE Trans. Energy Convers.*, 1997, **12**, (1), pp. 73–78
12 UTKIN, V.I.: 'Sliding mode control design principles and applications to electric drives', *IEEE Trans. Ind. Electronic.*, 1993, **40**, (1), pp. 23–36
13 ORTEGA, R., LORIA, A., SIRA-RAMIREZ, H., and NICKLASSON, P.: 'Passivity based control of Euler Lagrange systems' (Springer-Verlag, London, 1998, 1st edn.)
14 HO, E.Y.Y., and SEN, P.C.: 'Control dynamics of speed drive systems using sliding mode controller with integral compensation', *IEEE Trans. Ind. Appl.*, 1991, **27**, (5), pp. 883–892
15 SIRA-RAMIREZ, H., and RÍOS-BOLIVAR, M.: 'Feedback passivity of nonlinear multivariable systems'. Triennial World Congress of IFAC, IFAC'99, 1999, Beijing, China, pp. 73–78

10 Appendix A

GSIP nominal power:	5 KW
P:	28
R_s:	0.3676 Ω
L_q, L_d:	3.55 mH
ϕ_m:	0.2867 Wb
J:	7.856 Kg m^2
r:	1.84 m
R_b:	14 mΩ
C_b:	180 000 F
E_b:	48 V